MATERIALS SCIENCE

Nematic suspension of a microporous layered silicate obtained by forceless spontaneous delamination via repulsive osmotic swelling for casting high-barrier all-inorganic films

Patrick Loch[1], Dominik Schuchardt[1], Gerardo Algara-Siller[2,3], Paul Markus[1], Katharina Ottermann[1], Sabine Rosenfeldt[1], Thomas Lunkenbein[2], Wilhelm Schwieger[4], Georg Papastavrou[1], Josef Breu[1]*

Exploiting the full potential of layered materials for a broad range of applications requires delamination into functional nanosheets. Delamination via repulsive osmotic swelling is driven by thermodynamics and represents the most gentle route to obtain nematic liquid crystals consisting exclusively of single-layer nanosheets. This mechanism was, however, long limited to very few compounds, including 2:1-type clay minerals, layered titanates, or niobates. Despite the great potential of zeolites and their microporous layered counterparts, nanosheet production is challenging and troublesome, and published procedures implied the use of some shearing forces. Here, we present a scalable, eco-friendly, and utter delamination of the microporous layered silicate ilerite into single-layer nanosheets that extends repulsive delamination to the class of layered zeolites. As the sheet diameter is preserved, nematic suspensions with cofacial nanosheets of ≈9000 aspect ratio are obtained that can be cast into oriented films, e.g., for barrier applications.

INTRODUCTION

Layered or two-dimensional (2D) materials represent a versatile tool with a variety of properties. The pronounced anisotropy in bonding strength of layered solids like graphite (*1*), clay minerals (*2*), transition metal dichalcogenides (*3*), lepidocrite-type titanates (*4*), perovskite-type niobates (*5*, *6*), or $NaFeO_2$-typ cathode materials (*7*) leads to a platy morphology and, in many cases, to intracrystalline reactivity. The latter is frequently taken advantage of to increase the basal spacing and thus weaken the adhesion between layers. This then sets the stage for liquid-phase exfoliation by ultrasonic (US) treatment, which nowadays is established as the standard approach to produce nanosheets that are applied in a plethora of applications (*8*–*10*). Some applications like the formation of heterostructures (*11*), permselective microporous membranes (*12*), textured (barrier) films, or composites (*13*) require a uniform nanosheet thickness and a large aspect ratio (ratio of nanosheet diameter to thickness). US treatment clearly does not offer this degree of control as it inevitably leads to broad distribution of thicknesses and platelet breakage, thus the maximum aspect ratio inherent to the pristine platelet diameter will not be achieved (*8*, *9*).

Contrary to brute-force liquid-phase exfoliation, nanosheets of some charged layered materials may alternatively be obtained by thermodynamically allowed delamination via so-called repulsive osmotic swelling [see (*14*) for a definition of exfoliation versus delamination]. This was, however, long limited to a handful of layered compounds such as titanates (*15*, *16*), niobates (*5*, *6*), antimonates (*17*), manganese oxides (*18*), tungsten oxides (*19*), and clay minerals (*20*, *21*). The process resembles the dissolution of ionic crystals while being limited to one dimension because of the anisotropic bonding situation. In summary, osmotic swelling requires separation above a certain threshold value where entropic contributions of interlayer species convert the initial adhesion into repulsion. While this repulsive swelling is rare, many cases are known where solvation of pristine or exchanged interlayer cations leads to so-called crystalline swelling. In this swelling regime, uptake of solvent resembles a first-order phase transition and is limited to distinct values even in excess of swelling agent because the interaction of adjacent layers remains attractive (*21*). Although crystalline swelling weakens the adhesion in the ionic crystal, exfoliation is not a spontaneous process and requires external (shearing) forces. Exfoliation gives a broad distribution of multilayers aside of monolayers and because of the forces applied bears the risk of breaking platelets and thus reducing the aspect ratio. The ultimate defining signature for repulsive swelling is the formation of a liquid crystalline, nematic suspension of nanosheets, which is indicated by the presence of sharp reflections in its X-ray scattering patterns at small scattering angles, corresponding to large periodicities (*22*). The occurrence of a homogeneous and single liquid crystalline phase critically depends on the complete, thermodynamically driven delamination of the pristine crystallites in the solvent.

If the pristine platelets have appreciable diameters, even dilute suspensions obtained by repulsive osmotic swelling will not be isotropic. Rather, nematic liquid crystalline phases are formed because the rotation of nanosheets, which are separated to large distances (>10 nm) by swelling at low concentrations, is hindered (*21*, *23*, *24*). As no mechanical input is required for repulsive osmotic swelling, the process is most gentle and preserves the lateral extension of the parent crystal in the nanosheets, and hence, the aspect ratio is maximized. For (synthetic) clay minerals, spontaneous delamination into high–aspect ratio nanosheets has recently been extended to high–charge

[1]Bavarian Polymer Institute, Department of Chemistry, University of Bayreuth, Universitätsstraße 30, D-95447 Bayreuth, Germany. [2]Department of Inorganic Chemistry, Fritz-Haber-Institut der Max-Planck-Gesellschaft, Faradayweg 4-6, D-14195 Berlin, Germany. [3]Institute of Physics and IRIS Adlershof, Humboldt-Universität zu Berlin, D-12489 Berlin, Germany. [4]Institute of Chemical Reaction Engineering, Friedrich-Alexander University Erlangen-Nürnberg, Egerlandstraße 3, D-91058 Erlangen, Germany.
*Corresponding author. Email: josef.breu@uni-bayreuth.de

density vermiculite-type materials, and it was realized that bulky interlayer cations induce separation above the threshold separation distances and trigger delamination (*23*, *25*).

Compared to clay minerals, layered zeolites carry reactive silanol groups at the microporous basal surface, which renders zeolite nanosheets highly attractive for fabricating functional films and membranes (*26*–*29*). RUB-15 nanosheets, for example, were exfoliated by shear forces in a polymer melt and then used to cast into thin permselective membranes for hydrogen separation with a H_2/CO_2 selectivity of up to 100 (*12*). Alternatively, MCM-22P was already exfoliated following ion exchange with tetrapropylammonium hydroxide in water. The monolayer yield was 15 to 20%, and typical aspect ratios of ≈20 were observed (*30*). More recently, by ion exchange with tetrabutylammonium hydroxide (TBAOH) of MCM-56 and ZSM-55, aqueous dispersions of nanosheets were obtained with 40 and 70% yield, respectively, and typical aspect ratios of <200. Films of zeolite nanosheets could be casted following this approach (*27*, *31*).

Here, we present a scalable, eco-friendly, and utter delamination of ilerite (RUB-18) into nanosheets by repulsive osmotic swelling (Fig. 1A). As ilerite can easily be crystalized in quadratic plates of >6 μm diameter, upon its gentle delamination, nanosheets with exceptional aspect ratios (≈9000) are obtained. As a first example of its application potential, all-inorganic high-barrier films were fabricated by simply doctor-blading the nematic suspension.

RESULTS AND DISCUSSION

To trigger osmotic swelling, adjacent layers in a layered ionic crystal need to be separated by incorporation of solvent to a certain threshold value (*21*, *23*). At this stage, the translational entropy of the interlayer species (solvent and interlayer cations) becomes dominating over the electrostatic attraction of the negatively charged layers, and the interlayer cations and adjacent layers in the crystal repel each other. The threshold separation may be achieved only through the solvation enthalpy of interlayer cations, as is the case with clay minerals of low charge density like hectorite (*32*). For higher charge density, the threshold separation may still be achieved by supplementing hydration forces with a steric pressure exerted by bulky interlayer cations (*20*, *23*). The steric pressure arises once the equivalent area of the interlayer cation exceeds the charge density of the underlying anionic layer. While, for 2:1-type clay minerals like montmorillonite or hectorite, this charge density is permanent and independent of pH, for compounds like layered titanates (*33*, *34*) or zeolites (*35*, *36*), acidic OH groups are exposed at the basal surfaces and thus the charge density will alter with pH. For ilerite ($Na_8[Si_{32}O_{64}(OH)_8]\cdot 32\ H_2O$), only half of the acidic protons are replaced by Na^+ during crystallization. These interlayer cations can be readily exchanged by a hydrophilic and sterically demanding cationic amino sugar *N*-methyl-*D*-glucamonium (meglumine). As the organocation is a base, the charge density is modified concomitantly with the ion exchange.

Ilerite is a 2D microporous silica-based material with a layered structure built from [5^4] cages resembling the building units of zeolites. While each layer has a polar structure, the stacking is centrosymmetric. The layer charge originates from half of terminal silanol bonds being deprotonated at the pH of synthesis (pH 13) and is balanced by chains of edge sharing [$Na(H_2O)_6$] octahedra in the interlayer space (*37*). The single layer exhibits a network of four- and six-membered rings, making ilerite nanosheets potentially interesting for the fabrication of permselective hydrogen membranes (Fig. 1B). Ilerite grows as characteristic square-shaped platelets (Fig. 1C) with appreciable lateral extension (>6 μm).

Contrary to common layered zeolites [e.g., MFI (*29*), MCM-56 (*38*), or MCM-22 (*39*)], the synthesis of the microporous layered silicate ilerite requires no structural directing agent and can be performed under mild conditions (*40*–*42*). Phase-pure ilerite was obtained in a water-based sol-gel route by the simple mixing of NaOH pellets with H_2O and a colloidal SiO_2 dispersion in a defined molar ratio (Na_2O:SiO_2:H_2O ratio of 1:4:37) followed by annealing (4 weeks) at 100°C in a closed vessel. Upscaling of layered sodium silicates, in general, is straightforward and has been established in industry (Chemiekombinat Bitterfeld, CWK Bad Köstritz, and Hoechst AG). The moderate synthesis temperature of 100°C requires no high-pressure autoclaves; rather, the synthesis can be conducted in low-cost, closed, glassy carbon crucibles or stainless steel vessels. Phase purity of the synthesized ilerite was checked with powder X-ray diffraction (PXRD; Fig. 1D). The PXRD pattern could be completely indexed in space group $I4_1/amd$ (no. 141), indicating phase purity, and refinement of lattice parameters yielded $a = b = 7.333(3)$ Å and $c = 44.31(4)$ Å in accordance with Vortman *et al.* (*37*). The particle size was determined with static light scattering, resulting in a narrow particle size distribution and a median particle size of 6.7 μm (fig. S1).

As previously mentioned, quantitative delamination via repulsive delamination requires cation exchange with a bulky organocation like meglumine. The ternary amine is a strong base, allowing the exchange to be performed at high pH where the zeolite is perfectly stable and the base is still protonated. Simple ion exchange of interlayer Na^+ of the as-synthesized material with an aqueous solution of meglumine at pH 9 and subsequent reduction of the ionic strength gave nematic dispersions of ilerite monolayers (Fig. 1A).

In a typical procedure, the synthesized ilerite was repeatedly treated with a 1 M solution of meglumine in water to ensure a complete ion exchange of interlayer Na^+ with meglumine to obtain meglu-ilerite. The pH of the meglumine solution was adjusted to 9 by addition of HCl. Upon ion exchange, the basal spacing increased from 11.0 to approximately 14.9 Å (fig. S2). Ion exchange was complete and no residual interlayer Na^+ could be detected by energy-dispersive X-ray (EDX) spectroscopy (table S1). CHN analysis confirmed the intercalation of meglumine and was also used to calculate the amount of intercalated meglumine. Meglu-ilerite was found to contain 2.16 mmol/g of the organocation, which is notable less than the Na^+ content of the pristine ilerite (2.83 mmol/g). This indicates that, as expected at the lower pH of ion exchange, some silanol groups get protonated, resulting in a lowering of the charge density of the silicate layers. Nevertheless, the remaining charge density of meglu-ilerite is still high enough to generate steric pressure to assist expansion of the interlayer space beyond the threshold separation, as clarified when considering the charge equivalent areas. Meglumine has an equivalent area of 77 $Å^2$ per charge, which is larger than the charge density of the ilerite at pH 9 of 70 $Å^2$ per charge (for details of the calculation, see the Supplementary Materials). Neither the pristine ilerite nor other hydrophilic organocations like TBAOH, 2-ammonium-2-(hydroxymethyl)-1,3-propanediol, cyclohexylammonium, piperidine, 2-ammonium-3-(1H-imidazol-4-yl) propanoic acid (histidine), 2-(trimethylammonium)ethyl methacrylate, or 4-(dimethylammonium)pyridine allow for osmotic swelling because the hydration enthalpy is too low and the equivalent areas (table S2) are too small to take the basal spacing beyond the threshold separation.

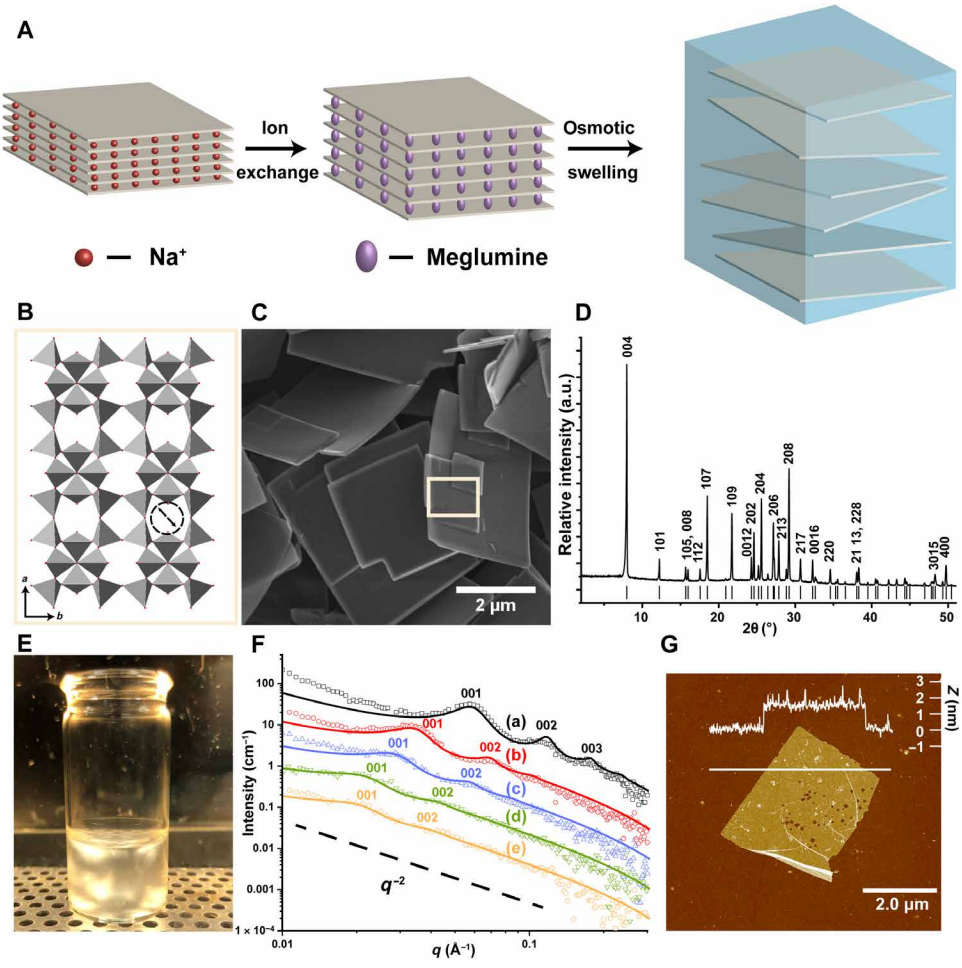

Fig. 1. Characterization and delamination of ilerite into nanosheets. (**A**) Schematic illustration of the delamination process by cation exchange of interlayer Na^+ against a bulky organocation meglumine and subsequent reduction of the ionic strength triggering osmotic swelling. (**B**) Structure of ilerite nanosheets. (**C**) Scanning electron microscopy (SEM) images of the pristine ilerite. Inset: The selected area of the structure. (**D**) Completely indexed PXRD pattern of ilerite indicating a phase pure material. Ticks indicate the theoretical reflections of ilerite. a.u., arbitrary units. (**E**) Nematic phase with characteristic birefringes formed upon delamination into nanosheets (0.5 volume %). (**F**) SAXS pattern proving complete delamination. Observed swelling upon addition of water to a highly concentrated gel with a solid content of 7.04 wt % (A) to 3.47 wt % (B), 2.81 wt % (C), 1.67 wt % (D), and 1.42 wt % (E), respectively. The corresponding *d*-spacings of 10.6, 18.0, 21.5, 28.5, and 30.0 nm, respectively, were obtained applying a simplified disc model. (**G**) Only single ilerite nanosheets could be found in the AFM with a characteristic square shape of the parent compound.

Because repulsive osmotic delamination is based on electrostatic repulsion, which is screened in ionic backgrounds, it tolerates only low ionic strengths (typically <0.02 M) (*21*). The ionic background was therefore lowered by repeated washing/centrifugation cycles or alternatively by dialysis. Both eventually triggered delamination of meglu-ilerite, and birefringent, nematic, aqueous suspensions consisting of zeolite-like silica-based monolayers could be obtained (Fig. 1E). Please note that, during washing/centrifugation, no coarse-grained, not delaminated material was discarded. The single-phase nature of the liquid crystal can easily be inspected by eye via a homogeneous birefringent appearance of the suspensions. The nanosheets in the nematic domains are separated to large distances, which are determined by the solid content of the suspensions. The separation of single nanosheets in a concentrated gel of 7.04 weight % (wt %) was determined by small-angle X-ray scattering (SAXS). Because of strong electrostatic repulsion, the negatively charged ilerite nanosheets adopt a cofacial arrangement (*21*, *24*) leading to a rational 00 *l* series in the SAXS pattern with a periodicity of 10.6 nm (Fig. 1F). The separation of 10.6 nm was obtained by fitting the scattering curve with a simplified disc model (for details, see fig. S3). Moreover, the observed q^{-2} scaling of the scattering intensity is typical for thin, platy scattering objects (*21*). The lack of basal reflections in the range of 1° to 10° 2θ, where ilerite and meglu-ilerite basal reflections would be expected, indicates complete delamination into monolayers (fig. S4).

Upon dilution of the highly concentrated gel, a continuous shift to lower *q* values was observed, indicating an increasing separation of the layers (Fig. 1F). The shift in the *d*-spacing from 10.7 to 30.0 nm corroborates the delamination mechanism that is based on repulsive osmotic swelling, because additional water is used to increase the distance between adjacent layers, minimizing the repulsive interactions of the negatively charged zeolite layers (*15*, *25*). While, for the highly concentrated gel, an intense 00 *l* series is clearly visible, the intensity decreases after further dilution. As previously observed for hectorite suspensions, upon increasing the separation distance, the thin and flexible nanosheets gradually loose the coplanarity by local undulations, etc. (*21*).

Quantitative conversion into high–aspect ratio monolayers was further confirmed with atomic force microscopy (AFM). For imaging, a highly diluted aqueous dispersion of ilerite was drop-casted on an ammonium modified Si wafer. For a single layer of ilerite, a height of 0.74 nm was calculated on the basis of the crystal structure of the parent compound. Because delaminated meglu-ilerite nanosheets have bulky, hydrated meglumine attached at the external surfaces, the height of 1.5 nm observed in AFM (fig. S5) is in good agreement with expectations and in line with the basal spacing of meglu-ilerite (Fig. 1G). Meglumine is slightly elliptical with an estimated diameter of 0.7 to 0.8 nm, adding to the nanosheet thickness of 0.74 nm. The nanosheet height of 1.5 nm observed with AFM (fig. S5) would therefore indicate a meglumine monolayer to be adsorbed only on the upper basal surface. On closer inspection of the AFM image, rectangular, nanoscopic holes become apparent. It is unclear whether they are inherited from defects in the pristine ilerite or whether they are etched into the nanosheets during the delamination. In any case, these represent pinholes that are expected to be detrimental to the barrier performance, as discussed later. Figure 1G and fig. S5 reveal another interesting feature: While crystalline ilerite is centrosymmetric, individual ilerite single-layer nanosheets have a polar structure meaning that the two basal surfaces are different. Ilerite nanosheets thus represent patchy platelets and consequently tend to roll up at the edges when cast on a planar support. This behavior tends to make preparation of AFM samples difficult and requires positively charged groups to be attached to the substrate surface by silylation.

To confirm the integrity of the structure of the ilerite monolayers, the nanosheets (fig. S6) were characterized with electron diffraction (ED) analysis. The experimentally observed diffraction pattern is in good agreement with simulated patterns of a single-layer ilerite, showing reflections at *d*-spacings of 7.32 and 5.18 Å [i.e., (100) and (110)]. These reflections are systematically absent in the ED pattern of the 3D bulk material (Fig. 2) because of the centrosymmetric stacking. Comparison of the ED pattern of a single-layer and a few-layer-thick bulk material, obtained by increasing the concentration, proves the sensitivity of ED to detect incomplete delamination or restacking. In particular, as the layer stacking in the bulk ilerite is centrosymmetric, reflection conditions imposed by the center of symmetry (i.e., *hk*0: *h*,*k* = 2n) are lifted for a single-layer nanosheet and reflections like 110 are observed (Fig. 2D). While the ED pattern of a single ilerite layer shows only discrete reflections, higher concentration of ilerite suspensions lead to a turbostratic restacking of monolayers resulting in an overlay of misoriented diffraction patterns from single layers, corroborating the successful delamination (fig. S7, A to C).

The obtained nanosheets are purely electrostatically stabilized without any steric contribution. Small molecular counter cations on the surface of the nanosheets can be easily replaced. Meglumine desorbs, for example, upon deposition of the nanosheets on the positively charged Si wafer from the bottom side of the surface. Moreover, because of the gentle delamination driven by thermodynamics, the large particle diameter of the parent ilerite may be transformed into an exceptional aspect ratio. Assuming the diameter of the parent ilerite as determined by light scattering to be preserved, the aspect ratio can be estimated (*32*). The height of the bare monolayers as found in the crystal structure is 0.74 nm, resulting in an estimated aspect ratio of more than 9000. Given this large aspect ratio, any type of casting on a planar substrate will inevitably result in textured, monodomain films with band-like structures formed because of partial overlap of adjacent nanosheets (Fig. 3A, inset). This renders ilerite most appropriate for applications such as barrier coatings. Liquid dispersions of the layered zeolite can easily be processed into highly oriented thin films applying common fabrication techniques like filtration, doctor blading, slot-die, or spray coating. In the following, we exemplify their high value in the field of barrier coatings. As the barrier improvement factor scales with the square of the aspect ratio, the gentle nature of repulsive osmotic delamination assuring maximum aspect ratios is key. The full potential inherent to the large diameter of the pristine ilerite crystals can be completely used because nanosheets are seldom broken during the delamination process.

Defect-free, thin ilerite films were obtained with doctor blading of a nematic nanosheet dispersion onto polyethylene terephthalate (PET) substrates (Fig. 3A). The casted film is optically clear, rendering it suitable for packaging of optoelectronic devices. EDX mapping of a film cross section shows the ilerite coating of ≈1.5 μm on the PET substrate (Fig. 3B and fig. S8). The high stacking order along the *c* axis of the nanosheets of the textured films is confirmed in the PXRD pattern, giving a basal spacing of 13.8 Å (Fig. 3C and fig. S9). Barrier performance of the coating was tested for H_2O, O_2, and He gases at a high relative humidity (r.h.) of 75% and 23°C for an ilerite

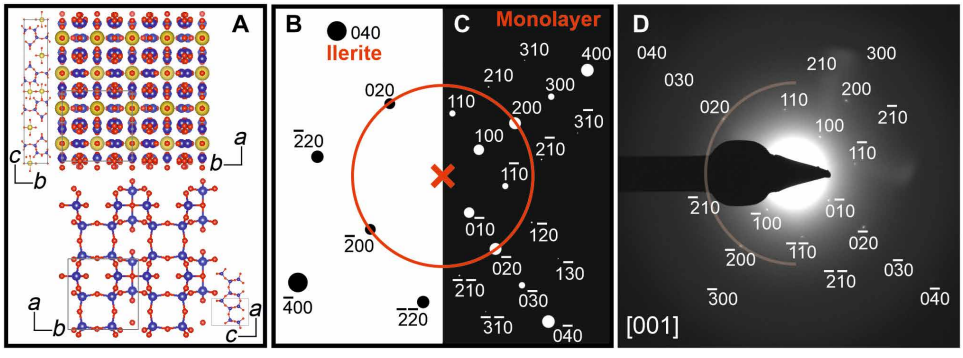

Fig. 2. ED analysis of ilerite nanosheets. (**A**) Structure of crystalline ilerite (top) and of a single layer (bottom) each displayed in two different orientations. (**B**) Simulated diffraction pattern of 3D crystalline ilerite compared to (**C**) a simulated diffraction pattern of a single-layer nanosheet of ilerite without Na^+ counter cations, both viewed perpendicular to the layer(s). Red circle marks the (200) reflection (i.e., 3.66-Å *d*-spacing) for comparison. (**D**) Experimental nanobeam ED pattern, with observed reflections, i.e., at 7.32 and 5.18 Å, corresponding to the reflections (100) and (110) in the simulated pattern of a single-layer ilerite. These reflections are absent with the centrosymmetric stacking of bulk ilerite. Width of diffraction patterns (B to D) is 10.17 nm^{-1} at 200 kV.

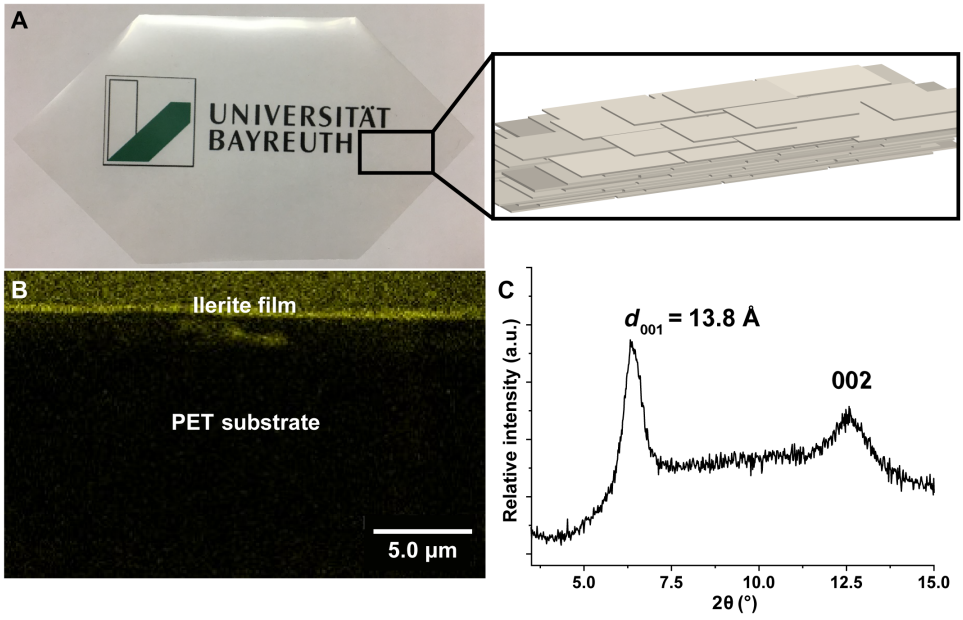

Fig. 3. Casting of thin zeolite films. (**A**) Doctor-bladed thin and clear ilerite film on a PET substrate, formed by overlapping, self-assembled coplanar ilerite nanosheets as schematically shown in the inset. (**B**) SEM image of a cross section of the film (1.5-µm thickness) with element mapping of Si. (**C**) Upon self-assembly, a 1D crystalline monodomain is obtained with a basal spacing of 13.8 Å as determined by PXRD.

film dried at 100°C. The water vapor transmission rate was below the detection limit (<0.05 g m^{-2} day^{-1}). For O_2 and He, transmission rates of 0.017 and 3.1 cm^3 m^{-2} day^{-1} atm^{-1}, respectively, were observed. Compared to the ilerite-coated substrate, the neat PET substrate shows a water vapor transmission rate of 4.42 g m^{-2} day^{-1} and O_2 and He transmission rates of 31.9 and 1740 cm^3 m^{-2} day^{-1} atm^{-1} (below 10% r.h.), respectively, confirming an excellent barrier performance of the inorganic film.

In conclusion, by establishing appropriate conditions for repulsive osmotic swelling, an environmentally friendly, water-born, and scalable process is introduced, producing functional zeolite-like nanosheets with 100% yield and a huge aspect ratio of ≈9000. By simple ion exchange of the layered parent zeolite-like layered silicate ilerite with an affordable, bulky amino sugar meglumine, nanosheets can be obtained quantitatively. The gentle nature of repulsive osmotic swelling preserves the lateral extensions of the parent crystal, as well as the crystal structure of single layers. Microporous, high–aspect ratio nanosheets are obtained that carry silanol groups on the basal surface allowing for further functionalization in future work. This makes ilerite nanosheets a highly promising material for various applications ranging from gas barrier applications to materials for permselective hydrogen membranes.

The process of repulsive osmotic swelling should generally work for charged layered compounds. Onset of repulsive osmotic swelling is triggered by the contribution of interlayer species to translational entropy and requires the interlayer gallery to be enlarged beyond a sufficient threshold. In most cases, solvation enthalpy is not sufficient to achieve this but needs to be supplemented by steric stress exerted by bulky interlayer cations. As layered zeolites carry acidic groups on the basal surfaces, the charge density is, however, dependent on the pH of the dispersion medium. The lower the pH, the lower the charge density will be and the bulkier the interlayer cation has to be to exert internal pressure. If amines are applied as interlayer cations, then the pH moreover is coupled to the pK_B value. As zeolites have a stability window in respect to low and high pH, identification of appropriate conditions for repulsive delamination might, in practice, turn out to be troublesome and require adjustment for every zeolite candidate. Last, materials to be delaminated must be truly 2D. Intergrown or self-intercalated structures will not work.

MATERIALS AND METHODS

Synthesis methods

Synthesis of ilerite

Ilerite was synthesized by applying a published procedure (*40*, *41*). Briefly, NaOH pellets (≥98%, Sigma-Aldrich) were dissolved in deionized water and added to colloidal SiO_2 (30 wt %, Köstrosol 1030 KD) under vigorous stirring, giving a molar Na_2O:SiO_2:H_2O ratio of 1:4:37. Typically, 99.85-g NaOH pellets (≥98%, Sigma Aldrich) were dissolved in 131.95-g deionized water and then added to 1000-g colloidal SiO_2. The layered zeolite was obtained after synthesis under hydrothermal conditions at 100°C for 4 weeks in a closed crucible. Ilerite was obtained in the form of a gel, washed with deionized water, and lastly dried in air.

Preparation of the colloidal dispersion

For preparation of the colloidal dispersion, ilerite was treated with an aqueous solution of meglumine (*N*-methyl-*D*-glucamine, >99.0%, Sigma-Aldrich). Before the treatment, meglumine was dissolved in deionized water, titrated to a pH of approximately 9 using HCl (32 wt %), and dissolved with purified water to yield a 1 M solution. Typically, 500 mg of the dried ilerite was suspended in 40 ml of a 1 M solution of meglumine, corresponding to a 28-fold excess of the cation exchange capacity (theoretically 284 meq/100 g). This treatment was repeated five times. The treated ilerite was separated from the liquid by centrifugation (10,000*g*, 10 min), and the supernatant solution was discarded and replaced by fresh 1 M solution of meglumine. Separation during the washing was performed by centrifugation (12,000*g*, 30 min). The obtained treated ilerite was washed with

deionized water to reduce the ionic strength, allowing the delamination into a delaminated layered zeolite dispersion as a gel.

Preparation of zeolite thin films

A layered zeolite dispersion, prepared as described above, was diluted to a concentration of approximately 2 wt %. Thin films of layered zeolite nanosheets were prepared by doctor blading on a PET foil using an automated device (Zehntner ZAA 2300, Zehntner GmbH Testing Instruments, Switzerland), followed by drying at 100°C in air.

Characterization

Powder X-ray diffraction

PXRD patterns were recorded in sealed glass capillaries on a STOE Stadi P powder diffractometer equipped with a MYTHEN1K detector using Cu $K_{\alpha 1}$ radiation (1.5406 Å). Textured samples were measured in Bragg-Brentano geometry on a PANalytical Empyrean diffractometer with Cu $K_{\alpha 1}$ radiation (λ = 1.5406 Å) equipped with a PixCel1D-Medipix3 detector.

Small-angle X-ray scattering

SAXS data of the gels were measured using a "Double Ganesha AIR" (SAXSLAB, Denmark). The X-ray source of this laboratory-based system is a rotating copper anode (MicroMax 007HF, Rigaku Corporation, Japan) providing a microfocused beam. The data were recorded by a position sensitive detector (PILATUS 300 K, Dectris). Samples of the treated layered zeolite were prepared by washing the meglumine-treated ilerite with a diluted aqueous solution of meglumine (0.05 M, pH 9) three times. The swelling experiment was conducted upon addition of a defined amount of ultrapure water to the highly concentrated gel. SAXS pattern is recorded after equilibration for 1 day in 1-mm glass capillaries. The circularly averaged data are normalized to incident beam, sample thickness, and measurement time. Background subtraction was performed by using the SAXS pattern of a water-filled capillary. Fitting of the scattering curve was performed by using the program scatter (version 2.5).

Atomic force microscopy

AFM was performed on a Bruker Dimension Icon, equipped with a NanoScope V controller. A ScanAsyst-Air silicon nitride tip (Bruker) was used in PeakForce mode. Samples were prepared by dropping a dilute aqueous dispersion (5 mg/liter) in Millipore water onto silicon wafers. The silicon wafers were cleaned with a snow jet, silylated with 3-(ethoxydimethylsilyl)propylamine via gas phase overnight and rinsed with ultrapure water prior application of the samples. The images were analyzed with a NanoScope Analysis 1.8 software.

Transmission electron microscopy

The samples for the electron microscopic characterization were prepared by dissolution in water, mixed thoroughly, and deposited on holey-carbon gold grids (Quantifoil Au 1.2-1.3). The prepared samples were then characterized in a transmission electron microscope (TEM) Titan 80-300 operated at 200 kV. The model structure of ilerite (*37*) was delaminated manually using the VESTA software (*43*). ED simulation was made using the software ReciPro taking kinematical and excitation error for intensity calculation.

Scanning electron microscopy and EDX spectroscopy

Scanning electron microscope images were recorded on a Zeiss 1530. Completeness of the ion exchange was checked with EDX on a Zeiss 1530 equipped with an EDX INCA 400 unit (Oxford) and a detection limit of 1 atomic %.

CHN analysis

An Elementar Unicode equipped with a combustion tube filled with tungsten (VI) oxide granules was used at a combustion temperature of 1050°C. Before the measurement, the delaminated gel of ilerite was freeze-dried, followed by drying at 80°C.

Gas permeation test

Oxygen transmission rates were determined applying a Mocon OX-TRAN 2/21 M10x instrument with a lower detection limit of 0.0005 $cm^3\ m^{-2}\ day^{-1}\ atm^{-1}$. A mixture of 95% N_2 and 5% H_2 was used as carrier gas, and pure O_2 (>99.95%, Linde Sauerstoff 3.5) was used as permeate gas. The measurement was conducted at 23°C and 75% r.h. Water vapor transmission rates were measured on a Mocon PERMATRAN-W Model 3/33 with a lower detection limit of 0.05 $g\ m^{-2}\ day^{-1}$ at 23°C and 75% r.h. Helium transmission rates were measured applying the pressure difference method with a gas transmission tester of Brugger Feinmechanik GmbH and a measurement limit of 0.5 $cm^3\ m^{-2}\ day^{-1}\ atm^{-1}$.

SUPPLEMENTARY MATERIALS

Supplementary material for this article is available at https://science.org/doi/10.1126/sciadv.abn9084

REFERENCES AND NOTES

1. D. D. L. Chung, Review graphite. *J. Mater. Sci.* **37**, 1475–1489 (2002).
2. E. Paineau, I. Bihannic, C. Baravian, A.-M. Philippe, P. Davidson, P. Levitz, S. S. Funari, C. Rochas, L. J. Michot, Aqueous suspensions of natural swelling clay minerals. 1. Structure and electrostatic interactions. *Langmuir* **27**, 5562–5573 (2011).
3. M. Chhowalla, H. S. Shin, G. Eda, L. J. Li, K. P. Loh, H. Zhang, The chemistry of two-dimensional layered transition metal dichalcogenide nanosheets. *Nat. Chem.* **5**, 263–275 (2013).
4. T. Tanaka, Y. Ebina, K. Takada, K. Kurashima, T. Sasaki, Oversized titania nanosheet crystallites derived from flux-grown layered titanate single crystals. *Chem. Mater.* **15**, 3564–3568 (2003).
5. W. Yang, S. Yamamoto, K. Sueyoshi, T. Inadomi, R. Kato, N. Miyamoto, Perovskite nanosheet hydrogels with mechanochromic structural color. *Angew. Chem. Int. Ed.* **60**, 8466–8471 (2021).
6. Y. Song, N. Iyi, T. Hoshide, T. C. Ozawa, Y. Ebina, R. Ma, S. Yamamoto, N. Miyamoto, T. Sasaki, Massive hydration-driven swelling of layered perovskite niobate crystals in aqueous solutions of organo-ammonium bases. *Dalton Trans.* **47**, 3022–3028 (2018).
7. J. Zhao, L. Zhao, N. Dimov, S. Okada, T. Nishida, Electrochemical and thermal properties of α-$NaFeO_2$Cathode for Na-Ion batteries. *J. Electrochem. Soc.* **160**, A3077–A3081 (2013).
8. J. N. Coleman, M. Lotya, A. O'Neill, S. D. Bergin, P. J. King, U. Khan, K. Young, A. Gaucher, S. De, R. J. Smith, I. V. Shvets, S. K. Arora, G. Stanton, H.-Y. Kim, K. Lee, G. T. Kim, G. S. Duesberg, T. Hallam, J. J. Boland, J. J. Wang, J. F. Donegan, J. C. Grunlan, G. Moriarty, A. Shmeliov, R. J. Nicholls, J. M. Perkins, E. M. Grieveson, K. Theuwissen, D. W. McComb, P. D. Nellist, V. Nicolosi, Two-dimensional nanosheets produced by liquid exfoliation of layered materials. *Science* **331**, 568–571 (2011).
9. V. Nicolosi, M. Chhowalla, M. G. Kanatzidis, M. S. Strano, J. N. Coleman, Liquid exfoliation of layered materials. *Science* **340**, 1226419 (2013).
10. R. J. Smith, P. J. King, M. Lotya, C. Wirtz, U. Khan, S. De, A. O'Neill, G. S. Duesberg, J. C. Grunlan, G. Moriarty, J. Chen, J. Wang, A. I. Minett, V. Nicolosi, J. N. Coleman, Large-scale exfoliation of inorganic layered compounds in aqueous surfactant solutions. *Adv. Mater.* **23**, 3944–3948 (2011).
11. A. K. Geim, I. V. Grigorieva, Van der Waals heterostructures. *Nature* **499**, 419–425 (2013).
12. M. Dakhchoune, L. F. Villalobos, R. Semino, L. Liu, M. Rezaei, P. Schouwink, C. E. Avalos, P. Baade, V. Wood, Y. Han, M. Ceriotti, K. V. Agrawal, Gas-sieving zeolitic membranes fabricated by condensation of precursor nanosheets. *Nat. Mater.* **20**, 362–369 (2020).
13. F. Ding, J. Liu, S. Zeng, Y. Xia, K. M. Wells, M.-P. Nieh, L. Sun, Biomimetic nanocoatings with exceptional mechanical, barrier, and flame-retardant properties from large-scale one-step coassembly. *Sci. Adv.* **3**, e1701212 (2017).
14. J. E. F. C. Gardolinski, G. Lagaly, Grafted organic derivatives of kaolinite: II. Intercalation of primary n-alkylamines and delamination. *Clay Miner.* **40**, 547–556 (2005).
15. T. Sasaki, M. Watanabe, Osmotic swelling to exfoliation. Exceptionally high degrees of hydration of a layered titanate. *J. Am. Chem. Soc.* **120**, 4682–4689 (1998).
16. F. Geng, R. Ma, Y. Ebina, Y. Yamauchi, N. Miyamoto, T. Sasaki, Gigantic swelling of inorganic layered materials: A bridge to molecularly thin two-dimensional nanosheets. *J. Am. Chem. Soc.* **136**, 5491–5500 (2014).
17. J.-C. P. Gabriel, F. Cemerel, B. J. Lemaire, H. Desvaux, P. Davidson, P. Batall, Swollen liquid-crystalline lamellar phase based on extended solid-like sheets. *Nature* **413**, 504–508 (2001).

18. Y. Omomo, T. Sasaki, L. Wang, M. Watanabe, Redoxable nanosheet crystallites of MnO2 derived via delamination of a layered manganese oxide. *J. Am. Chem. Soc.* **125**, 3568–3575 (2003).
19. K. Fukuda, K. Akatsuka, Y. Ebina, R. Ma, K. Takada, I. Nakai, T. Sasaki, Exfoliated nanosheet crystallite of cesium tungstate with 2D pyrochlore structure: Synthesis, characterization, and photochromic properties. *ACS Nano* **2**, 1689–1695 (2008).
20. G. F. Walker, Macroscopic swelling of vermiculite crystals in water. *Nature* **187**, 312–313 (1960).
21. S. Rosenfeldt, M. Stöter, M. Schlenk, T. Martin, R. Q. Albuquerque, S. Förster, J. Breu, In-depth insights into the key steps of delamination of charged 2D nanomaterials. *Langmuir* **32**, 10582–10588 (2016).
22. P. Davidson, C. Penisson, D. Constantin, J. P. Gabriel, Isotropic, nematic, and lamellar phases in colloidal suspensions of nanosheets. *Proc. Natl. Acad. Sci. U.S.A.* **115**, 6662–6667 (2018).
23. M. Daab, N. J. Eichstaedt, C. Habel, S. Rosenfeldt, H. Kalo, H. Schießling, S. Förster, J. Breu, Onset of osmotic swelling in highly charged clay minerals. *Langmuir* **34**, 8215–8222 (2018).
24. K. Sano, Y. S. Kim, Y. Ishida, Y. Ebina, T. Sasaki, T. Hikima, T. Aida, Photonic water dynamically responsive to external stimuli. *Nat. Commun.* **7**, 12559 (2016).
25. M. Daab, N. J. Eichstaedt, A. Edenharter, S. Rosenfeldt, J. Breu, Layer charge robust delamination of organo-clays. *RSC Adv.* **8**, 28797–28803 (2018).
26. K. Varoon, X. Zhang, B. Elyassi, D. D. Brewer, M. Gettel, S. Kumar, J. A. Lee, S. Maheshwari, A. Mittal, C.-y. Sung, M. Cococcioni, L. F. Francis, A. V. Mccormick, K. A. Mkhoyan, M. Tsapatsis, Dispersible exfoliated zeolite nanosheets and their application as a selective membrane. *Science* **334**, 72–75 (2011).
27. W. J. Roth, T. Sasaki, K. Wolski, Y. Song, D.-M. Tang, Y. Ebina, R. Ma, J. Grzybek, K. Kalahurska, B. Gil, M. Mazur, S. Zapotoczny, J. Cejka, Liquid dispersions of zeolite monolayers with catalytic activity prepared by soft-chemical exfoliation. *Sci. Adv.* **6**, eaay8163 (2020).
28. K. V. Agrawal, B. Topuz, T. C. Pham, T. H. Nguyen, N. Sauer, N. Rangnekar, H. Zhang, K. Narasimharao, S. N. Basahel, L. F. Francis, C. W. Macosko, S. Al-Thabaiti, M. Tsapatsis, K. B. Yoon, Oriented MFI membranes by Gel-Less secondary growth of sub-100 nm MFI-nanosheet seed layers. *Adv. Mater.* **27**, 3243–3249 (2015).
29. M. Choi, K. Na, J. Kim, Y. Sakamoto, O. Terasaki, R. Ryoo, Stable single-unit-cell nanosheets of zeolite MFI as active and long-lived catalysts. *Nature* **461**, 246–249 (2009).
30. T. Maluangnont, Y. Yamauchi, T. Sasaki, W. J. Roth, J. Cejka, M. Kubu, The aqueous colloidal suspension of ultrathin 2D MCM-22P crystallites. *Chem. Commun.* **50**, 7378–7381 (2014).
31. W. J. Roth, T. Sasaki, K. Wolski, Y. Ebina, D. M. Tang, Y. Michiue, N. Sakai, R. Ma, O. Cretu, J. Kikkawa, K. Kimoto, K. Kalahurska, B. Gil, M. Mazur, S. Zapotoczny, J. Cejka, J. Grzybek, A. Kowalczyk, Exfoliated ferrierite-related unilamellar nanosheets in solution and their use for preparation of mixed zeolite hierarchical structures. *J. Am. Chem. Soc.* **143**, 11052–11062 (2021).
32. M. Stöter, D. A. Kunz, M. Schmidt, D. Hirsemann, H. Kalo, B. Putz, J. Senker, J. Breu, Nanoplatelets of sodium hectorite showing aspect ratios of ≈ 20,000 and superior purity. *Langmuir* **29**, 1280–1285 (2013).
33. R. Ma, T. Sasaki, Nanosheets of oxides and hydroxides: Ultimate 2D charge-bearing functional crystallites. *Adv. Mater.* **22**, 5082–5104 (2010).
34. L. Wang, T. Sasaki, Titanium oxide nanosheets: Graphene analogues with versatile functionalities. *Chem. Rev.* **114**, 9455–9486 (2014).
35. W. J. Roth, O. V. Shvets, M. Shamzhy, P. Chlubná, M. Kubů, P. Nachtigall, J. Čejka, Postsynthesis transformation of three-dimensional framework into a lamellar zeolite with modifiable architecture. *J. Am. Chem. Soc.* **133**, 6130–6133 (2011).
36. W. J. Roth, B. Gil, W. Makowski, B. Marszalek, P. Eliášová, Layer like porous materials with hierarchical structure. *Chem. Soc. Rev.* **45**, 3400–3438 (2016).
37. S. Vortmann, J. Rius, S. Siegmann, H. Gies, Ab initio structure solution from X-ray powder data at moderate resolution: Crystal structure of a microporous layer silicate. *J. Phys. Chem. B* **101**, 1292–1297 (1997).
38. B. Gil, W. Makowski, B. Marszalek, W. J. Roth, M. Kubu, J. Cejka, Z. Olejniczak, High acidity unilamellar zeolite MCM-56 and its pillared and delaminated derivatives. *Dalton Trans.* **43**, 10501–10511 (2014).
39. V. V. Narkhede, H. Gies, Crystal structure of MCM-22 (MWW) and its delaminated zeolite ITQ-2 from high-resolution powder x-ray diffraction data: An analysis using rietveld technique and atomic pair distribution function. *Chem. Mater.* **21**, 4339–4346 (2009).
40. G. Borbély, H. K. Beyer, H. G. Karge, W. Schwieger, A. Brandt, K. H. Bergk, Chemical characterization, structural features, and thermal behavior of sodium and hydrogen octosilicate. *Clays Clay Miner.* **39**, 490–497 (1991).
41. W. Schwieger, K.-H. Bergk, Dehydrierung und hydrogenolyse an Metallpolysilicathydraten. *Z. Chem.* **25**, 228–230 (1985).
42. P. Loch, T. Martin, M. Grüner, G. Kaupp, W. Schwieger, J. Breu, Synthesis of large platelets of egyptian blue via pseudomorphosis after NaRUB-18. *Z. anorg. allg. Chem.* **646**, 1570–1574 (2020).
43. K. Momma, F. Izumi, *VESTA* 3 for three-dimensional visualization of crystal, volumetric and morphology data. *J. Appl. Cryst.* **44**, 1272–1276 (2011).

Acknowledgments: We appreciate the support of the Keylab for Optical and Electron Microscopy of the Bavarian Polymer Institute and for providing access to SAXS facilities within the Keylab Mesoscale Characterization: Scattering Techniques. We thank M. Schwarzmann and U. Mansfeld for collecting EDX spectra and SEM images. O. Khoruzhenko is acknowledged for the graphic design and R. Timmins for English proofreading. We thank X. Duan and K.-V. Agrawal for fruitful discussion on membranes. **Funding:** G.A-S. acknowledges funding support of the Deutsche Forschungsgemeinschaft (DFG; German Research Foundation) (Projektnummer: 451037016) (PReGrAM). P.L. thanks Elite Network Bavaria in the framework of the Elite Study Program "Macromolecular Science" for support. This work was funded by the Deutsche Forschungsgemeinschaft (DFG; German Research Foundation) (491183248) and by the Open Access Publishing Fund of the University of Bayreuth. **Author contributions:** J.B. conceived and supervised the research. P.L. conceived the research and established the synthesis and delamination. W.S. gave valuable assistance with synthesis. D.S. casted barrier films and measured transmission rates. G.A.-S. and T.L. took TEM images and ED patterns. P.M., K.O., and G.P. performed and interpreted AFM images. S.R. measured and fitted the SAXS data. P.L., D.S., G.A.-S., and J.B. wrote the manuscript. All authors discussed the results and commented on the manuscript. **Competing interests:** P.L. and J.B. have applied for a patent (application number EP20205796.4) entitled "Process for delamination of layered zeolite, a delaminated layered zeolite dispersion and use thereof." The authors declare that they have no other competing interests. **Data and materials availability:** All data needed to evaluate the conclusions in the paper are present in the paper and/or the Supplementary Materials.

Submitted 29 December 2021
Accepted 1 April 2022
Published 18 May 2022
10.1126/sciadv.abn9084

ScienceAdvances

Nematic suspension of a microporous layered silicate obtained by forceless spontaneous delamination via repulsive osmotic swelling for casting high-barrier all-inorganic films

Patrick LochDominik SchuchardtGerardo Algara-SillerPaul MarkusKatharina OttermannSabine RosenfeldtThomas LunkenbeinWilhelm SchwiegerGeorg PapastavrouJosef Breu

Sci. Adv., 8 (20), eabn9084. • DOI: 10.1126/sciadv.abn9084

Science Advances (ISSN) is published by the American Association for the Advancement of Science. 1200 New York Avenue NW, Washington, DC 20005. The title *Science Advances* is a registered trademark of AAAS.